JOURNAL OF THERMOPHYSICS AND HEAT TRANSFER
Vol. 13, No. 1, January–March 1999

Permeability Impact on the Pressure Rise in a Pultrusion Die

K. S. Raper,* J. A. Roux,† J. G. Vaughan,‡ and E. Lackey‡
University of Mississippi, University, Mississippi 38677

The pressure rise in a pultrusion die inlet can have a significant impact on the quality of a pultruded product; therefore, a model to predict the pressure rise would be a very useful and effective tool for enhancing the pultrusion process and the pultruded product. There are several parameters that can strongly affect the pressure rise in the pultrusion die inlet. One particular parameter is the permeability. In this study, three permeability models are employed to investigate their effect on the pressure rise in the pultrusion die inlet. A numerical model, based on Darcy's law for flow in a porous media that employs the finite volume solution method, is developed to predict the pressure and velocity fields in the pultrusion die. The numerical results are compared with some preliminary experimental data for both glass and graphite composites to determine which permeability model agrees best with the data. An effective fiber diameter is introduced to account for nonuniform fiber diameters and nonuniform spatial fiber distributions.

Nomenclature

C = Kozeny constant
C_L = total axial length of computational domain, m
D_e = effective fiber diameter, m
D_f = fiber diameter, m
D_L = length from start of straight portion to end of computational domain, m
H_D = die half thickness, m
H_P = preform plate half thickness, m
$h(x)$ = distance from centerline to tapered die wall, m
K_{11} = permeability in axial direction, m^2
K_{22} = permeability in transverse direction, m^2
L = length from intersection point to start of straight portion, m
$\dot{m}$ = forward mass flow rate, kg/s
P = pressure, Pa
P_0 = inflow boundary pressure, 101,325 Pa
R_C = radius of curvature of tapered die inlet, m
R_f = fiber radius, m
T = temperature, K
T_L = axial length of tapered region, m
U = fiber velocity in axial direction, m/s
u = resin velocity in axial direction, m/s
V = fiber velocity in transverse direction, m/s
V_f = fiber volume fraction of the finished product
V_{f_0} = initial fiber volume fraction from computational domain inlet to intersection point
$V_f(x)$ = local fiber volume fraction
v = resin velocity in transverse direction, m/s
W = width or unit width of die cavity, m
x = axial coordinate
y = vertical coordinate
α = local die wall taper angle
μ = viscosity of liquid resin, kg/m s
ρ = density of liquid resin, kg/m^3
φ = porosity of fiber bundle
ψ = degree of cure

Received Dec. 3, 1997; revision received Aug. 24, 1998; accepted for publication Oct. 8, 1998.

*Graduate Student, Department of Mechanical Engineering.
†Faculty, Department of Mechanical Engineering. Senior Member AIAA.
‡Faculty, Department of Mechanical Engineering.

Introduction

THE pultrusion process for manufacturing composite materials has become increasingly important because it is one of the most cost-effective ways to produce high strength-to-weight ratio materials that are used extensively in high-performance aircraft and spacecraft. A schematic of the pultrusion process is shown in Fig. 1. The process of pultrusion involves a few simple, but vital components, which include fiber reinforcement, a resin impregnation tank, preform plates, a heated die, a puller, and a cutoff saw. The focus of this study is to predict the pressure rise in the pultrusion die inlet while employing various permeability models to model the flow of resin through the fiber matrix. The permeability can be defined as the measure of the ease with which the resin diffuses through the fiber bundle. The permeability models employed by the numerical model are used to predict the flow of resin through the fiber bundle both isotropically and anisotropically. The permeability will have a significant impact on the die inlet pressure rise; therefore, it is very important to accurately predict the flow of resin through the fiber bundle. A significant pressure rise can help suppress void formations and promote good fiber wet out; this, in turn, impacts the quality of the part being manufactured. Thus, a model to predict the pressure rise would be a very useful tool for enhancing the pultrusion process and improving the quality of the pultruded product. Very little work has been published on the pressure rise in the pultrusion die inlet. Batch and Macosko[1] were the first to investigate the pressure rise in the tapered region of the die. They developed a one-dimensional fluid flow model based on Darcy's law, but the closed-form solution did not yield realistic velocity profiles. Gorthala et al.[2] developed a two-dimensional model in cylindrical coordinates based on the hydrodynamic theory of lubrication for the tapered entrance region of the die. Valliappan[3] developed a two-dimensional model in Cartesian coordinates based on the hydrodynamic theory of lubrication. Sharma et al.[4] developed a more complete analysis of the pressure rise in the tapered inlet region of the die. Based on Darcy's law of flow in a porous media, Sharma et al. employed the finite element method to solve for the pressure as a function of various process control parameters. In Sharma et al.'s research, only one permeability model was employed in which the permeability was modeled isotropically.

To separate this work from other works,[1–4] various anisotropic permeability models were employed as well as more comprehensive boundary conditions than utilized by Sharma et al. For this particular study, the Kozeny–Carman[5] permeability model (used by Sharma et al.), the Gebart[6] permeability

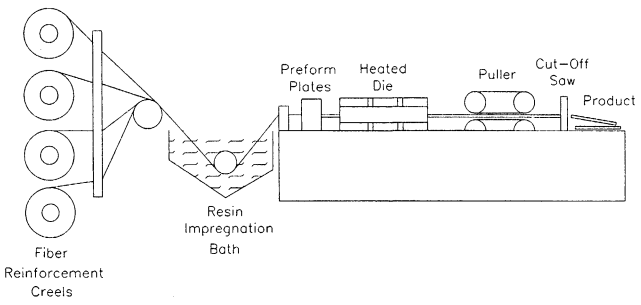

Fig. 1 Schematic of the pultrusion process.

model, and the Gutowski et al.[7] permeability model were employed to predict the pressure and velocity fields in the pultrusion die. The present study is a numerical investigation that utilizes the finite volume method[8] to aid in selecting appropriate process control parameters, geometric parameters for pultrusion die inlets, and various permeability models that will establish a better foundation for enhancing the pultrusion process. The numerical results are compared with some preliminary experimental data to determine which permeability model best agrees with the data.

Statement of Problem

In this study, the pressure rise is referred to as the difference between the initial pressure (1 atm) and the increase in pressure as the resin and fiber bundle are compressed from the final preform plate cavity thickness to the die cavity thickness. Figure 2 depicts the resin and fiber bundle as they enter the pultrusion die. Here, glass and graphite composites of 0.00318-m (1/8-in.) thick cross sections are simulated to predict the pressure rise in the pultrusion die inlet as a function of the various permeability models. These predictions are then compared with preliminary experimental data. Because the pressure rise is symmetric about the centerline, only the top half is modeled. As the resin and fiber bundle are pulled through the tapered region of the die inlet, a significant rise in pressure occurs. This distinct pressure rise occurs because the resin and fiber bundle are being compressed from the final preform plate cavity half thickness, H_P, down to the half thickness of the straight portion of the die, denoted as H_D. As the resin and fiber bundle are being compressed, excess resin (shown by the small arrows in Fig. 2) is squeezed from the system resulting in a rapid rise in pressure. Note that in this study the preform cavity plate thickness is taken as $1.20H_D$.

The length from the start of the computational domain inflow boundary to the straight portion of the die is designated as the tapered length (T_L) and is taken to be 6 mm (0.24 in.). The point where the fibers make contact with the tapered boundary is referred to as the intersection point. The distance from the intersection point to the start of the straight portion of the die is designated as L, which is a function of the preform plate half thickness, H_P, and geometry of the die inlet contour. The length D_L, which is the length of the die straight portion that is modeled, is taken as 406.4 mm (16 in.). The total length of the computational domain is designated as C_L, and is taken to be 412 mm (16.24 in.). The computational domain outflow boundary is just beyond the point of gelation at a distance C_L from the computational domain inlet. Gelation is referred to as the point where the resin begins to cure or solidify, causing the liquid resin viscosity to rise rapidly to very high values. It is this sudden rise in the resin viscosity that causes the pressure rise to decrease back to essentially zero.

The viscosity model (presented later) from the work of Gorthala et al.[2] is employed to obtain the viscosity profile in the straight portion of the die. The temperature and degree of cure profiles for different pull speeds and fiber volume fractions were obtained from the work of Chachad[9] and Chachad et al.[10] The viscosity varies as a function of the temperature and degree of cure, which, in turn, are functions of the axial distance x caused by the placement of resistance cartridge heaters along the die length for a Pultrusion Technology Inc. (PTI) model Pulstar 804 pultruder.

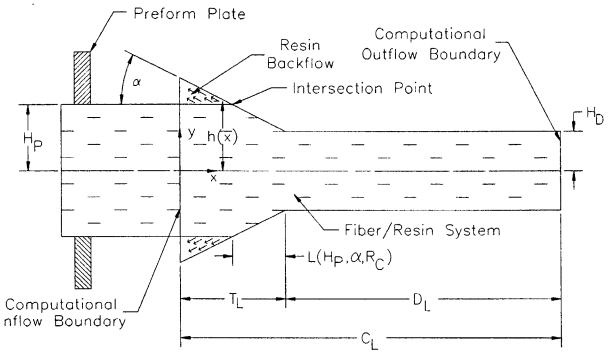

Fig. 2 Schematic of the computational domain for the study.

Mathematical Model

The governing equations for Darcy's flow are given as follows:

x-momentum equation:

$$u = -\frac{K_{11}}{\mu\phi}\frac{\partial P}{\partial x} \tag{1a}$$

y-momentum equation:

$$v = -\frac{K_{22}}{\mu\phi}\frac{\partial P}{\partial y} \tag{1b}$$

Continuity equation:

$$\frac{\partial(\phi u)}{\partial x} + \frac{\partial(\phi v)}{\partial y} = 0 \tag{2}$$

Equation (1a) corresponds to the x component of the resin velocity in the liquid region or the backflow region above the intersection line. Equation (1b) corresponds to the velocity of the resin in the y direction, starting from the computational domain inlet up to the intersection point, and also, from the start of the straight portion to the computational domain outlet. The x component of the resin velocity in the entire region below and including the intersection line (within the composite) is represented by

$$u = U - \frac{K_{11}}{\mu\phi}\frac{\partial P}{\partial x} \tag{3a}$$

From the intersection point up to the start of the straight portion of the die, the y component of the resin velocity is represented by

$$v = V - \frac{K_{22}}{\mu\phi}\frac{\partial P}{\partial y} \tag{3b}$$

where V is the y component of the of the fiber velocity, which can be written as

$$V = -U[y/h(x)]\tan\alpha \tag{3c}$$

To economize the numerical technique, a single equation based on the field variable pressure P is obtained, which has three different forms, depending on which region of the computational domain is being considered. For example, the equa-

tion for the region above the intersection line can be obtained by substituting Eqs. (1a) and (1b) into Eq. (2), which yields

$$\frac{\partial}{\partial x}\left(\frac{K_{11}}{\mu}\frac{\partial P}{\partial x}\right) + \frac{\partial}{\partial y}\left(\frac{K_{22}}{\mu}\frac{\partial P}{\partial y}\right) = 0 \tag{4a}$$

For the regions below and including the intersection line that are upstream of the intersection point, and also, after the start of the straight portion of the die downstream to the outflow boundary, the governing equation can be obtained by substituting Eqs. (3a) and (1b) into Eq. (2)

$$\frac{\partial}{\partial x}\left(\frac{K_{11}}{\mu}\frac{\partial P}{\partial x}\right) + \frac{\partial}{\partial y}\left(\frac{K_{22}}{\mu}\frac{\partial P}{\partial y}\right) = U\frac{\partial \phi}{\partial x} \tag{4b}$$

The last equation that corresponds to the region between the intersection point and the start of the straight portion of the die is obtained by substituting Eqs. (3a) and (3b) into Eq. (2)

$$\frac{\partial}{\partial x}\left(\frac{K_{11}}{\mu}\frac{\partial P}{\partial x}\right) + \frac{\partial}{\partial y}\left(\frac{K_{22}}{\mu}\frac{\partial P}{\partial y}\right) = U\left[\frac{\partial \phi}{\partial x} - \frac{\phi}{h(x)}\tan\alpha\right] \tag{4c}$$

Viscosity Model

The viscosity is assumed to be constant from the computational domain inlet up to the straight portion of the die. After entering the straight portion of the die, the viscosity varies as a function of the temperature and degree of cure. The viscosity model[2] used in this study is given as

$$\mu = \mu_\infty \exp\{[E/RT(x)] + k\psi(x)\} \tag{5}$$

where $E = 3.76 \times 10^4$ J/mol and $k = 45.0$. In this study, viscosity profiles corresponding to the EPON 9420/9470 epoxy resin system were employed. For a viscosity measurement of 1.5 kg/m s at standard temperature and pressure (STP), the corresponding value for μ_∞ was determined to be 5.12×10^{-7} kg/m s. The values of $T(x)$ and $\psi(x)$ in Eq. (5) were obtained from the work of Chachad[9] and Chachad et al.[10] The temperature field in the tapered die inlet is constant; thus, the resin degree of cure in the inlet is zero because no reaction has been initiated yet. In the die straight region (see Fig. 2) the $T(x)$ and $\psi(x)$ profiles were input from the work of Chachad[9] and Chachad et al.[10]; their work solved the energy and species equations simultaneously and considered the flowfield to be slug flow. The slug flow consideration is a reasonable one in the die straight region because this is essentially what Darcy's equations yield for a pultrusion die; this is a consequence of the velocity slip condition at the die wall [Eq. (12b)], which is consistent and required for solving Darcy's equations. However, because the momentum and energy equations were not solved simultaneously in this work, the results do contain a degree of approximation; this approximation is better for thin composites than for thick composites.

Permeability Models

The numerical model is capable of using three different permeability models. These three models were employed to predict how the pressure field behaves as a result of differences in the axial permeability, the transverse permeability, and different fiber arrangements. The first model, the Kozeny–Carman equation,[5] which was used by Sharma et al.,[4] predicts the permeability in the axial direction as follows:

$$K_{11} = \frac{D_f^2}{16C}\frac{(1 - V_f)^3}{V_f^2} \tag{6}$$

Sharma et al. used a value of 1.4 for the constant C in Eq. (6), as recommended by Batch and Macosko.[1] Also, Sharma et al. chose $D_f = 15$ μm. In this study, two different fiber types, which include glass (PPG 2001 112 yield) and graphite (AS4 12K), are considered. The Kozeny–Carman[5] model assumes that the permeability in the transverse direction is the same as the permeability in the axial direction; therefore, $K_{22} = K_{11}$.

Table 1 Numerical values of the parameters in Eqs. (7) and (8)

Fiber arrangement	C_1	$V_{f_{max}}$	c
Quadratic	0.4	0.7853	57
Hexagonal	0.231	0.9068	53

The second model is taken from the work of Gebart.[6] For the Gebart permeability model, a quadratic or hexagonal fiber arrangement can be employed. The numerical model is capable of using either type of fiber arrangement. Gebart models the permeability in the axial direction as

$$K_{11} = \frac{8R_f^2}{c}\frac{(1 - V_f)^3}{V_f^2} \tag{7}$$

The permeability in the transverse direction is given as

$$K_{22} = C_1[\sqrt{(V_{f_{max}}/V_f)} - 1]^{5/2}R_f^2 \tag{8}$$

where numerical values for parameters C_1, $V_{f_{max}}$, and c in Eqs. (7) and (8) are given in Table 1.

The third model is taken from the work of Gutowski et al.[7] The permeability in the axial direction is the same as the Kozeny–Carman[5] model given in Eq. (6). The permeability in the transverse direction is given as

$$K_{22} = \frac{1}{4k'}\frac{(\sqrt{(V_a'/V_f)} - 1)^3}{(V_a'/V_f) + 1}R_f^2 \tag{9}$$

where V_a' and k' are empirical parameters taken as 0.76 and 0.20, respectively, for a quadratic fiber arrangement. For hexagonal fiber arrangement, V_a' and k' were taken to be 0.907 and 0.20, respectively.

Fiber Volume Fraction and Porosity

The fiber volume fraction referenced in this study is the fiber volume fraction of the finished product (die straight portion). It should be noted that the fiber volume fraction before the intersection point is different from that of the straight portion of the die; the fiber volume fraction from the computational domain inlet up to the intersection point is given by

$$V_{f_0} = V_f(H_D/H_P) \tag{10}$$

From the intersection point to the straight portion, the fiber volume fraction increases as a function of the decreasing cross-sectional area from the initial value V_{f_0} to the fiber volume fraction V_f, which is specified for the finished product. Another important area of consideration is the all-liquid resin backflow region that lies above the fiber/resin system between the inflow boundary and the intersection point. The fiber volume fraction in this region was taken as 0.001, which is the value used by Sharma et al.[4] Although this region contains no fibers, because of computational problems, the fiber volume fraction could not be given a value of zero. The porosity of the fiber bundle within the entire computational domain is taken as

$$\phi(x) = [1 - V_f(x)] \tag{11}$$

Boundary Conditions

The boundary conditions for the governing equations in terms of the pressure and velocities are as follows:

$$P = P_0 \quad \text{at} \quad x = 0 \tag{12a}$$

$$\tan\alpha = -v/u \quad \text{at} \quad y = h(x) \tag{12b}$$

$$v = 0 \quad \text{at} \quad y = 0 \tag{12c}$$

$$u = U \quad \text{at} \quad x = C_L \tag{12d}$$

For the tapered wall, the boundary condition is taken from the local angle α, which is the angle the tapered die wall makes with the horizontal. In terms of the components of the velocities in both the x and y directions, the boundary condition [Eq. (12b)] is obtained; note Eq. (12b) can also be obtained by requiring the normal component of the resultant velocity at the wall to be zero (no penetration into wall). At the computational domain outlet, the x component of the velocity is equal to the pull speed of the pultrusion process. This assumption can be implemented because at the computational domain outlet, the fiber/resin system is essentially a solid and the liquid pressure rise has returned to zero as a result of the rapid rise in the viscosity of the resin and the transition of the porous media into a solid nonporous media. Note that Eq. (12a) will remain the same. Transforming the velocity boundary conditions [Eqs. (12b–12d)] into pressure boundary conditions via Eqs. (1a), (1b), and (3a–3c), yields the following for the computational domain:

$$\frac{K_{11}}{\mu}\frac{\partial P}{\partial x}\sin\alpha + \frac{K_{22}}{\mu}\frac{\partial P}{\partial y}\cos\alpha = 0 \quad \text{at} \quad y = h(x) \tag{13a}$$

$$\frac{\partial P}{\partial y} = 0 \quad \text{at} \quad y = 0 \tag{13b}$$

$$\frac{\partial P}{\partial x} = 0 \quad \text{at} \quad x = C_L \tag{13c}$$

The finite volume method[8] is employed to solve for the pressure from Eqs. (4a–4c). Once the pressure field is obtained, a finite difference method is employed to determine the velocity fields from Eqs. (1a), (1b), (3a), and (3b). A total of 3370 nodes were employed for the grid of the computational domain. On average, the computational time of the numerical model is approximately 30 s on a Pentium® Pro 200 MHz personal computer with 128 MB of RAM.

Results and Discussion

Comparison of Permeability Models

Three permeability models were employed to predict the pressure rise in the pultrusion die inlet. The Kozeny–Carman[5] model given in Eq. (6) assumes that the permeability is isotropic ($K_{11} = K_{22}$), whereas the Gebart[6] model, Eqs. (7) and (8), and the Gutowski et al.[7] model, Eqs. (6) and (9), consider $K_{11} \neq K_{22}$. The Kozeny–Carman and Gutowski models both use the same equation for the permeability in the axial direction (K_{11}), whereas the Gebart model employs Eq. (7) to obtain K_{11}. Using Eq. (7) of the Gebart model reduces the value of K_{11} ~15.5% when compared with K_{11} obtained by Eq. (6) of the Kozeny–Carman and Gutowski models for a given fiber diameter. All three models employ different expressions to obtain the permeability in the transverse direction (K_{22}). Using the Gebart [Eq. (8)] or Gutowski [Eq. (9)] permeability models will reduce the value of K_{22} ~5 and 20 times, respectively, as compared with the Kozeny–Carman value, [Eq. (6)], for a given fiber diameter. These models were chosen so that the pressure field in the pultrusion die inlet could be investigated when the permeability is modeled isotropically and anisotropically.

To best illustrate the pressure rise predicted by the numerical model, the centerline pressure rise is presented as a function of the axial distance along the die. For this case study, the nominal values of the process control parameters (see Fig. 3) for glass (PPG 2001 112 yield) fibers (D_f = 24 μm) are employed. A radius curvature of 0.00635 m (1/4 in.) was employed for the tapered region of the die inlet contour. Also note that the parameters used to model the permeability are the recommended values taken from the literature[6,7] for the three permeability models. Figure 3 illustrates the predicted pressure rise in the tapered region (reduced scale) of the die inlet (from the computational domain inlet up to the start of the straight portion), whereas Fig. 4 illustrates the predicted centerline pressure rise over the entire (expanded scale) axial length of the computational domain for the three permeability models. The Gutowski/quadratic model yielded the highest pressure rise, while the Kozeny–Carman model yielded the lowest pressure rise of the three permeability models. These results would suggest that because there is very little change

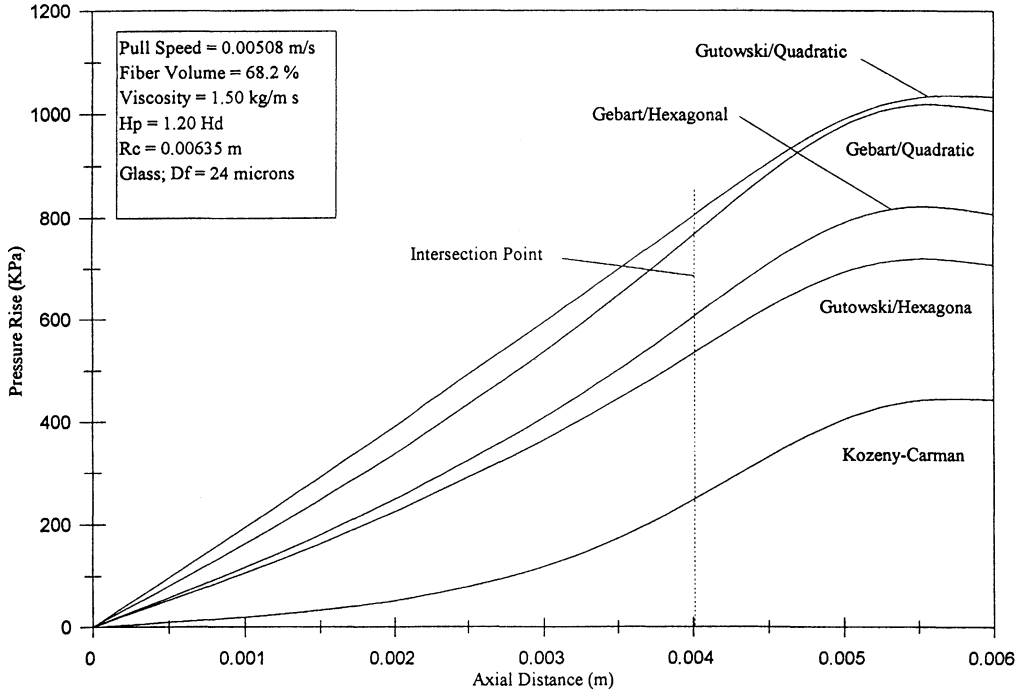

Fig. 3 Centerline pressure rise in the tapered inlet region for various permeability models.

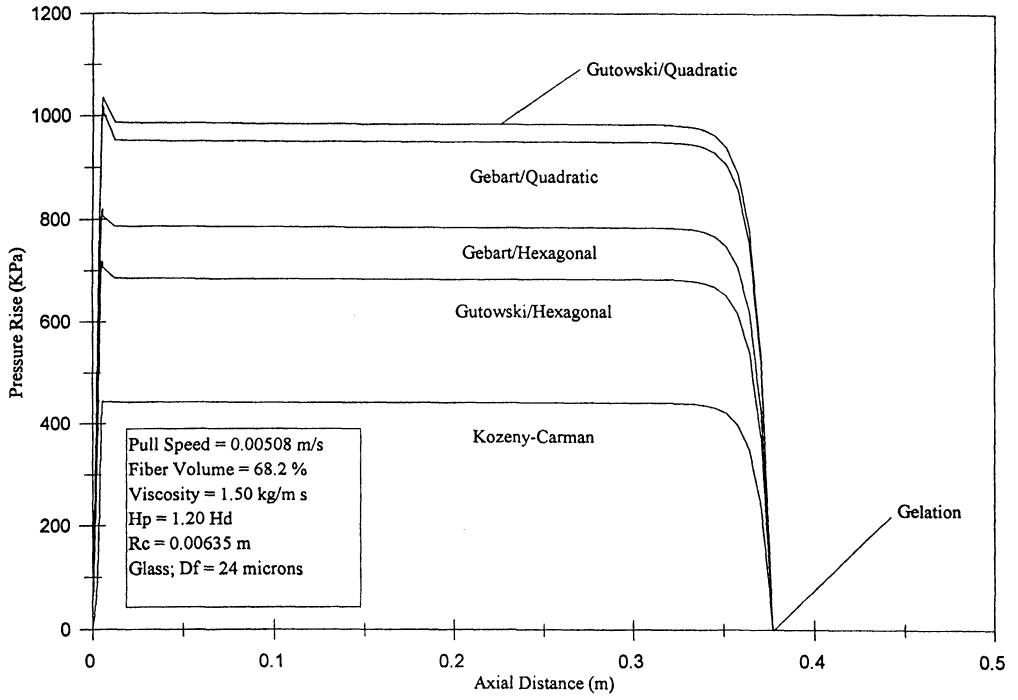

Fig. 4 Centerline pressure rise for the computational domain for various permeability models.

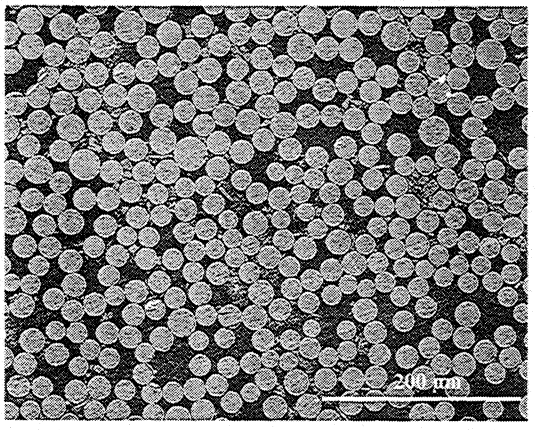

Fig. 5 Typical fiber arrangement and fiber diameter distribution for glass fibers.

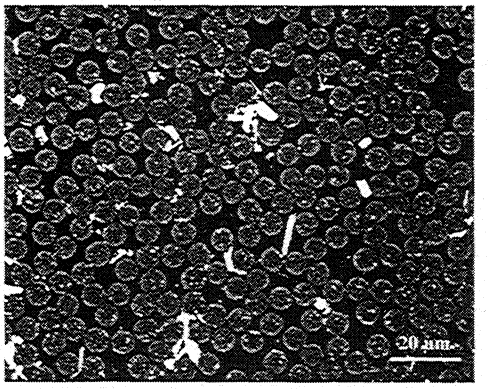

Fig. 6 Typical fiber arrangement and fiber diameter distribution for graphite fibers.

in the value K_{11} compared with K_{22} for the three permeability models, the value of K_{22} has the stronger impact on the pressure rise in the pultrusion die inlet. Decreasing K_{22} results in an increase in the die inlet pressure rise. As illustrated in Fig. 4, the pressure rises sharply at the die inlet with a slight peak in pressure just before the straight portion of the die, and then holds essentially steady throughout the straight portion until the resin cures. Once the resin starts to cure, the pressure rise decreases to zero because of the rapidly increasing viscosity; this point is referred to as the gelation point (refer to Fig. 4). Gelation is defined here as the point where the resin rapidly transforms (viscosity rapidly increases) from the liquid phase toward the solid phase.

Comparison of Numerical Results to Preliminary Experimental Data

Before comparing results with experimental data, it is useful to show the fiber distribution over a cross-sectional area for both glass and graphite composites. Typical fiber distributions for glass and graphite composites can be seen in Figs. 5 and 6, respectively. For glass composites, the fiber diameter varies in size from ~15–30 μm, and the spatial fiber distribution is clearly not uniform. Because the model assumes a constant fiber diameter, the fiber diameter was taken to be 24 μm for glass fibers. For the graphite composite, the size of the fibers is fairly uniform at approximately 7.5 μm, but the fiber distribution as shown in Fig. 6 is clearly not spatially uniform. As shown in these two figures, some fibers are touching while others are not, leaving large areas open to fluid flow. Because some fibers are touching, it is necessary to introduce an effective fiber diameter (D_e) to compensate for the large gaps between the fibers and the illusion of a larger fiber diameter. Gebart[6] and Gutowski et al.[7] introduced an effective D_e to match their experimental permeability data. The reason for employing an effective fiber diameter is because the permeability models all assume uniform fiber sizes and uniform fiber spacing, which is clearly (Figs. 5 and 6) not the actual case; thus, one might refer to the use of an effective fiber diameter as rendering the models to being somewhat semiempirical.

Some experimental pressure rise data were available so that a comparison could be made to investigate which permeability model most closely agrees with the data. Experimental pressure rise data corresponding to SHELL EPON® 9420 glass

composites for the following two pultrusion process runs were available.:

$U = 0.00508$ m/s (12 in./min), $\mu = 1.50$ kg/m s, $V_f = 66.1\%$

$U = 0.00762$ m/s (18 in./min), $\mu = 1.50$ kg/m s, $V_f = 66.1\%$

Also, some pressure data were available for SHELL EPON® 9420 graphite composites for the processing conditions listed next:

$U = 0.00508$ m/s (12 in./min), $\mu = 1.50$ kg/m s, $V_f = 62.1\%$

$U = 0.00508$ m/s (12 in./min), $\mu = 1.50$ kg/m s, $V_f = 64.4\%$

The experimental pressure rise data were measured for the PTI model Pulstar 804 pultruder at the University of Mississippi's Materials Science Laboratory. For the glass composites, Curite™ sensors were used to measure the pressure rise as the fiber/resin system entered the die. The Curite™ sensor is a strain gauge-type sensor approximately 15.4 mm wide and 0.32 mm thick. For the graphite composites, a Photonetics 1450 fiber-optic pressure probe ~0.8 mm in diameter was employed to measure the pressure rise in the pultrusion die inlet. A circular contoured die inlet with a radius (R_C) of curvature of 0.00635 m (0.25 in.) for a 0.0254 m × 0.003175 m (1 in. × 1/8 in.) finished product was used during the process of measuring the pressure rise. For the numerical model, the initial resin viscosity (pot resin) was taken to be 1.50 kg/m s; values between 1.50 and 3.0 kg/m s are reasonable values for the epoxy resin viscosity used here. The fiber diameter (D_f) for glass fibers was taken to be 24 μm and the fiber volume was taken to be 66.1% to match the experimental test conditions.

Inputting these values into the numerical model, the predicted pressure rise in the pultrusion die inlet did not agree with the experimental data for any of the permeability models. For this reason, an effective fiber diameter (D_e)[6,7] for each model was employed to better match the numerical predictions with the experimental data. An effective glass fiber diameter (D_e) of 20, 26, 29, 25, and 30 μm was used to better match the numerical model with the experimental data for the Kozeny–Carman,[5] Gebart/hexagonal,[6] Gebart/quadratic,[6] Gutowski/hexagonal,[7] and Gutowski/quadratic[7] permeability models, respectively. The die straight portion pressure rise was modeled for each permeability and compared to the experimental pressure rise for the glass composites (see Table 2). Using an effective fiber diameter allowed all of the permeability models to agree with the experimental data with very reasonable results for the glass composites. One important feature to point out is that both the numerical model and the preliminary experimental data show that an increase in pull speed results in an increase in the die pressure rise.

Preliminary experimental pressure data were also available to compare with the numerical results for SHELL EPON® 9420 graphite composites. The graphite fiber diameter was measured (see Fig. 6) to be approximately 7.5 μm. Using this fiber diameter (7.5 μm) resulted in unreasonably large pressure rises. Again, an effective fiber diameter was used to better match the predicted pressure rise with the experimental data. The D_e used to match the numerical results to the experimental

Table 2 Comparison of numerical data from permeability models to experimental data for fiberglass/EPON® 9420

Condition	Effective glass fiber diameter, μm	Maximum pressure rise, kPa $U = 0.00508$ m/s (12 in./min) $\mu = 1.50$ kg/m s $V_f = 66.1\%$	Maximum pressure rise, kPa $U = 0.00762$ m/s (18 in./min) $\mu = 1.50$ kg/m s $V_f = 66.1\%$
Kozeny–Carman[5]	20	523 (75.8 psi)	784 (114 psi)
Gebart/hexagonal[6]	26	551 (79.9 psi)	827 (120 psi)
Gebart/quadratic[6]	29	525 (76.1 psi)	788 (114 psi)
Gutowski/hexagonal[7]	25	516 (74.8 psi)	775 (112 psi)
Gutowski/quadratic[7]	30	502 (72.8 psi)	754 (109 psi)
Experimental	N/A	450 (65 psi)	862 (125 psi)

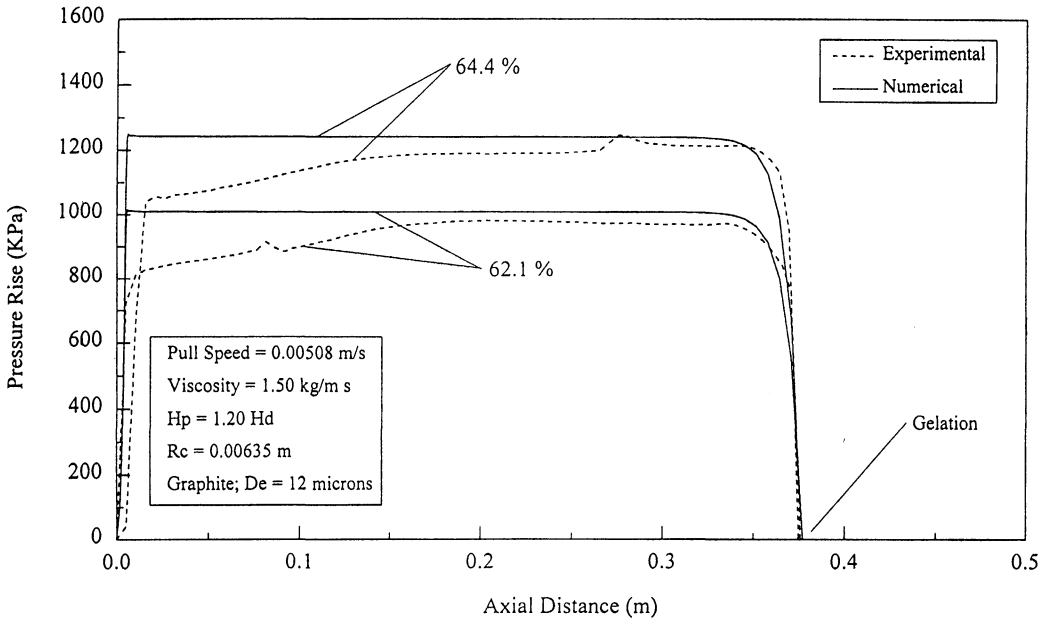

Fig. 7 Numerical vs experimental for the Kozeny–Carman[5] permeability model.

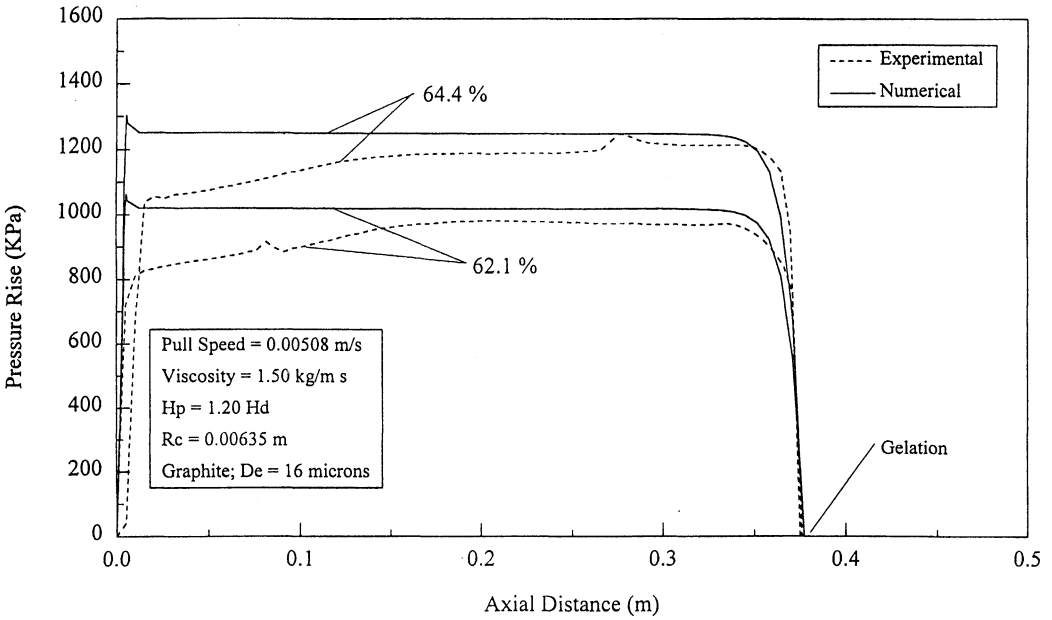

Fig. 8 Numerical vs experimental for the Gebart/hexagonal permeability model.

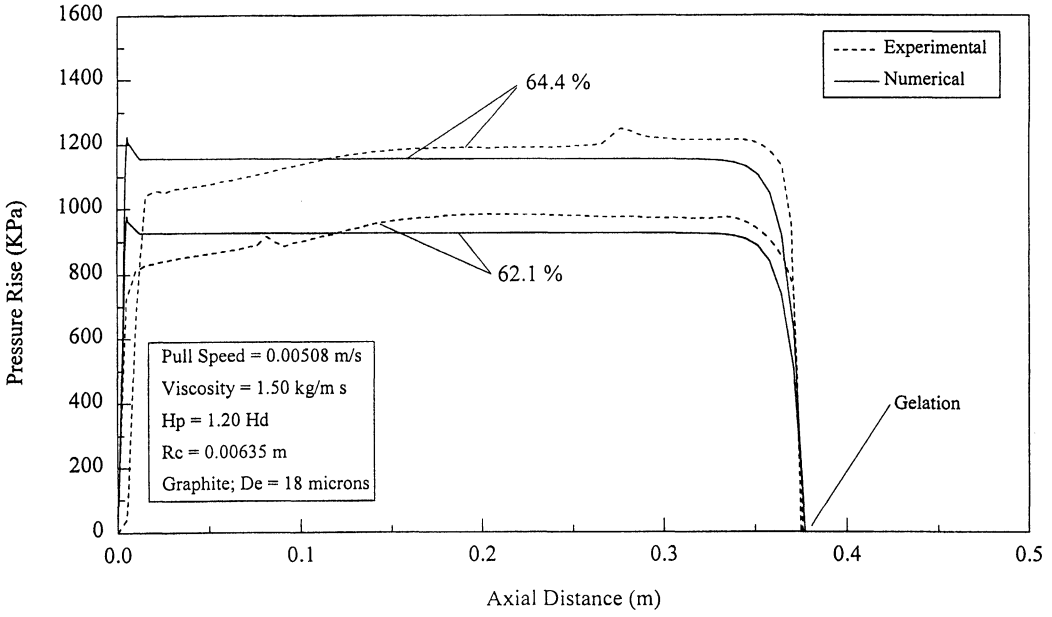

Fig. 9 Numerical vs experimental for the Gebart/quadratic permeability model.

data for Kozeny–Carman,[5] Gebart/hexagonal,[6] Gebart/quadratic,[6] Gutowski/hexagonal,[7] and Gutowski/quadratic[7] permeability models were 12, 16, 18, 15, and 18 μm, respectively. The predicted pressure rise and the preliminary data are plotted over the axial distance of the die up to the point of gelation for all the permeability models for the two fiber volume fractions. The predicted pressure rise compared with the experimental data for the Kozeny–Carman, Gebart/hexagonal, Gebart/quadratic, Gutowski/hexagonal, and Gutowski/quadratic permeability models can be seen in Figs. 7, 8, 9, 10, and 11, respectively. All of the permeability models predict the pressure rise as a function of the fiber volume fraction for graphite fibers with very reasonable agreement when compared with the preliminary experimental data. As shown in these five figures, the numerical model predicted the gelation point with remarkable accuracy when compared with the gelation point of the preliminary experimental data. Even the effect of the pressure rise rolling off from the plateau was captured by the numerical model. Here again, it is noteworthy that the numerical model and the preliminary experimental data both show that an increase in the fiber volume will result in an increase in the die inlet pressure rise.

The question now is which permeability model most accurately predicts the pressure rise in the pultrusion die inlet. To answer this question, the pros and cons of each permeability model must be considered, because an effective fiber diameter can be used to achieve reasonable agreement with the experimental data. The Kozeny–Carman[5] permeability models $K_{11} = K_{22}$, whereas the Gebart[6] and Gutowski[7] model $K_{11} \neq K_{22}$. Realistically, the permeability (K_{22}) in the transverse direction will not equal the permeability (K_{11}) in the axial direction.[6,7] For this reason, the Kozeny–Carman permeability model will not be selected. Also, as shown in Figs. 5 and 6, the fiber arrangement tends to be more hexagonal than quadratic, and so the quadratic fiber arrangements for both the Gebart[6] and the Gutowski[7] models were not selected. Both the Gebart/hexagonal[6] and the Gutowski/hexagonal[7] permeability models agreed equally well with the experimental data when an effec-

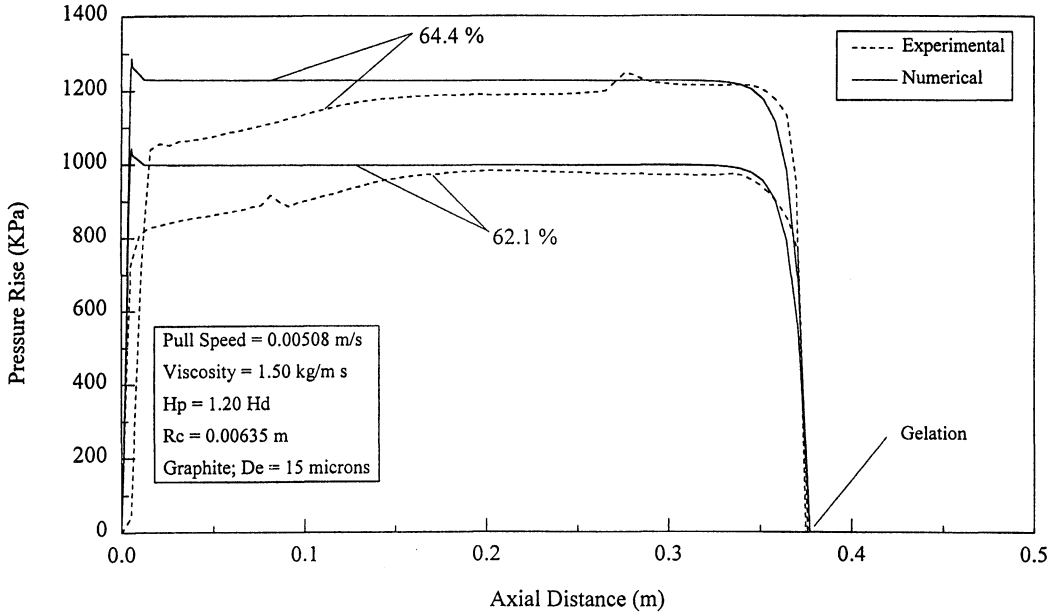

Fig. 10 Numerical vs experimental for the Gutowski/hexagonal permeability model.

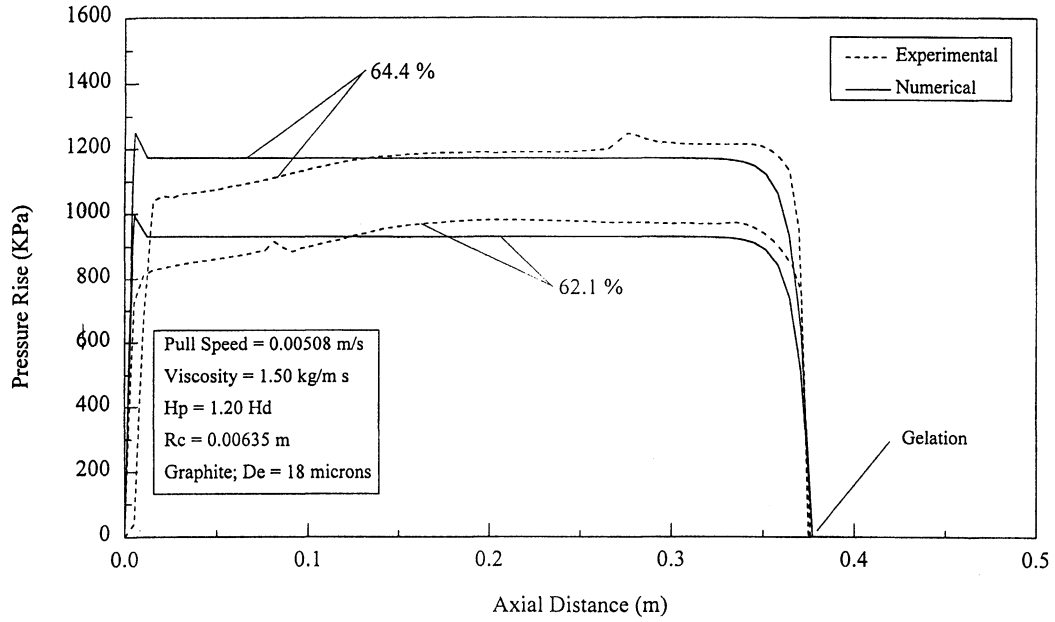

Fig. 11 Numerical vs experimental for the Gutowski/quadratic permeability model.

tive fiber diameter was employed. Therefore, either model could be used to predict the pressure rise in the pultrusion die inlet to obtain reasonable results when compared with experimental data.

Not only is the pressure rise in the pultrusion die an important aspect of this study, but also the velocity field predicted by the numerical model can yield important information. In Fig. 12, the Gebart/hexagonal[6] permeability model is used to show a velocity vector field, which illustrates the flow pattern of the resin through the computational domain. Figure 12 shows only a selected region of the computational domain concentrating on the area around the intersection point. The backflow in the liquid region above the fiber bundle system can be seen in the velocity vector field. As Fig. 12 illustrates, the backflow does not extend past the intersection point. The resin velocity vectors inside the fiber bundle are being turned upward near the intersection point. After the intersection point, the resin velocity vectors are being forced downward along the converging die wall boundary. The shape of the flow pattern, i.e., the resin flow occurring with the velocity component transverse to the fiber direction, would suggest that the enhanced fiber wetout is occurring near the intersection point of Fig. 12.

To ensure that the pressure and velocity fields are accurate, a quality-control check generated by the numerical model was employed. The quality-control check generated by the numerical model is based on the overall mass flow rate through the die. For the pressure and velocity fields predicted by the numerical model to be accurate and valid solutions, the overall mass flow rate determined by the numerical model must agree with the theoretical overall mass flow rate. The overall mass flow rate generated by the numerical model was compared with the theoretical mass flow ($\rho U H_D W \varphi_s$) rate at each axial location along the die for both the Gebart/hexagonal[6] and the Gutowski/hexagonal[7] permeability models. The overall mass flow rate as computed by the numerical model and the theoretical mass flow rate for both permeability models agreed with very good accuracy. It was determined that the maximum per-

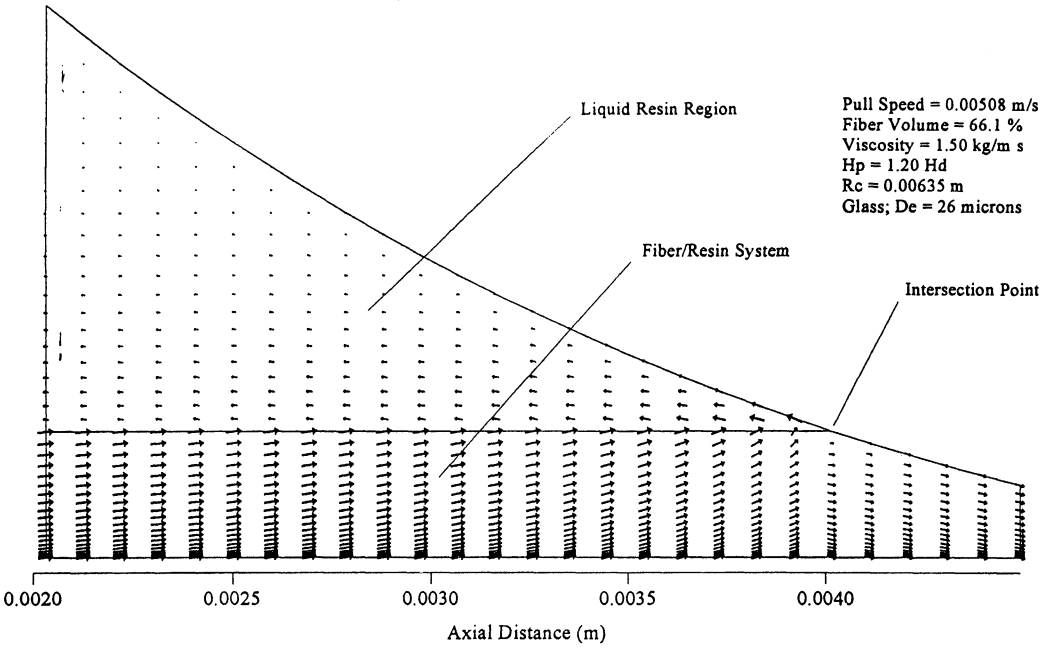

Fig. 12 Velocity vector field for the Gebart/hexagonal permeability model.

cent error between the overall theoretical mass flow rate and the numerical mass flow rate was less than 0.5%.

Conclusions

A numerical model that employed the finite volume solution method, based on Darcy's law of fluid (resin) flow through a porous (fibrous) medium, was developed to obtain the resin pressure and resin velocity fields in a pultrusion die. The model is capable of employing either an isotropic or anisotropic permeability model to simulate the fluid flow. The results of the numerical model were compared with some preliminary experimental pressure rise data. An effective fiber diameter was introduced to better match the experimental data that does render the model to be somewhat semiempirical. Once the effective fiber diameter was employed, the comparisons of the numerical results with the experimental data were very reasonable for all of the permeability models investigated. It is believed that the permeability in the transverse direction will not equal the permeability in the axial direction; therefore, the Kozeny–Carman[5] permeability model was not chosen to simulate the fluid flow. Also, based on cross sections of the glass and graphite fiber composites, it appears that the fiber arrangement tends to be somewhat more hexagonal than quadratic; therefore, the quadratic fiber arrangement was not considered. Both the Gebart/hexagonal[6] and Gutowski/hexagonal[7] permeability models agreed reasonably well with the experimental data. Either permeability model could be used to simulate the flow of the resin to obtain an accurate pressure rise in the pultrusion die inlet.

Acknowledgments

This research was supported by National Science Foundation Grant EPS-9452857 and the University of Mississippi.

References

[1]Batch, G. L., and Macosko, C. W., "Analysis of Pressure, Pulling Force, and Sloughing in Pultrusion," *Proceedings of the AIAA/ASME 5th Thermophysics and Heat Transfer Conference*, AIAA, Washington, DC, 1990.

[2]Gorthala, R., Roux, J. A., and Vaughan, J. G., "Impact of Pultrusion Pull Speed on Temperature and Degree of Cure Profiles Within a Composite Material," *Proceedings of the 46th Annual Conference*, Composites Institute, SPI, Inc., 1991, pp. 13-D/1-5.

[3]Valliappan, M., "Thermal, Flow, and Cure Characterization of Pultruded Circular Composites," Ph.D. Dissertation, Univ. of Mississippi, University, MS, 1996.

[4]Sharma, D., McCarty, T. A., Roux, J. A., and Vaughan, J. G., "Investigation of Dynamic Pressure Behavior in a Pultrusion Die," *Journal of Composite Materials*, Vol. 32, No. 10, 1998, pp. 929–951.

[5]Carman, P. C., "Fluid Flow Through Granular Beds," *Trans. Int. Chem. Eng.*, Vol. 15, 1939, pp. 150–160.

[6]Gebart B. R., "Permeability of Unidirectional Reinforcements for RTM," *Journal of Composite Materials*, Vol. 26, Aug. 1992, pp. 1100–1133.

[7]Gutowski, T. G., Cai, Z., Bauer, S., Boucher, D., Kingery, J., and Wineman, S., "Consolidation Experiments for Laminate Composites," *Journal of Composite Materials*, Vol. 21, July 1987, pp. 650–669.

[8]Patankar, S. V., *Numerical Heat Transfer and Fluid Flow*, Hemisphere, New York, 1980.

[9]Chachad, Y. R., "Thermal Characterization for Three Dimensional Irregular Shaped Graphite and Fiberglass Epoxy Based Pultruded Composites," Ph.D. Dissertation, Univ. of Mississippi, University, MS, 1995.

[10]Chachad, Y. R., Roux, J. A., Vaughan, J. G., and Arafat, E. S., "Three-Dimensional Characterization of Pultruded Fiberglass-Epoxy Composite Materials," *Journal of Reinforced Plastics and Composite Materials*, Vol. 14, No. 5, 1995, pp. 495–513.